Protic Ionic Liquids Based Crosslinked Polymer Electrolytes: A New Class of Solid Electrolytes for Energy Storage Devices

Energy Technology
Generation, Conversion, Storage, Distribution
www.entechnol.de



# Protic Ionic Liquids-Based Crosslinked Polymer Electrolytes: A New Class of Solid Electrolytes for Energy Storage Devices

*Timo Stettner, Gabriele Lingua, Marisa Falco, Andrea Balducci,* and Claudio Gerbaldi**

**Herein, the preparation of an innovative crosslinked polymer electrolyte (PEO_HPyr) encompassing protic ionic liquids (PILs) displaying high ionic conductivity, wide thermal, and electrochemical stability is reported, thus suitable for use in safe energy storage devices. The first example of an all-solid-state electrochemical double layer capacitor (EDLC) containing a PEO_HPyr-based electrolyte is presented, which shows high performance at ambient temperature and exceptional stability. Furthermore, the first example of a PIL-based lab-scale lithium-metal cell with lithium iron phosphate cathodes is also presented, which provides almost full capacity (i.e., 150 mAh $g^{-1}$ at C/20) and highly reversible cycling at ambient conditions and different current rates. The excellent results obtained clearly demonstrate that PIL-based crosslinked polymer electrolytes represent a new and very interesting class of solid electrolytes for energy storage devices.**

## 1. Introduction

Protic ionic liquids (PILs) are a subgroup of ionic liquids (ILs) characterized by the presence of an acidic proton in their structure. PILs display the typical properties of ILs, including high thermal stability and low flammability, with the advantage of being easily synthesized through simple acid-base reactions.[1] Although less popular than aprotic ionic liquids (AILs), PIL-based electrolytes have been considered in energy applications for many years. Initially, PILs have been mainly used as electrolytes for fuel cells.[2] Afterward, their use as electrolytes in electrochemical capacitors has been investigated, and, only recently, they have been proposed as electrolytes for Li-ion batteries (LIBs).[3] In the last couple of years, their use in Na ion as well as K-ion batteries has also been considered.[1c,4] The results of these studies indicate that PIL-based electrolytes allow the realization of alkali metal-ion batteries with promising performances. Furthermore, they showed that the acidic proton in the structure of PILs could be advantageously used to tune the ion environment and the storage process dynamics taking place in these devices. It has been shown, for example, that the presence of this proton is favorably influencing the coordination of $Li^+$ ions in LIBs, making PILs suitable for high-power applications.[5] Finally, it has also been shown that aqueous solutions containing high concentration of PILs, which can be indicated as "water-in-PIL" electrolytes, display unique properties and are acting like aprotic and protic electrolytes at the same time.[6]

It is evident that the properties of PILs and PIL-based electrolytes are strongly influenced by the acidic proton and by the environment in which the proton is present. Dry PILs (with a water content lower than 50 ppm) display transport and thermal properties comparable to that of AILs. However, the presence of the acidic proton limits the electrochemical stability window (ESW) of PILs, making it significantly lower compared with that of AILs.[7] In spite of this, it has been shown that the use of film forming additives decomposing within the ESW of PILs enables the use of carbonaceous anodes, e.g., graphite and hard/soft carbon, in combination with PIL-based electrolytes.[8]

To date, a large number of investigations have been dedicated to polymer electrolytes based on room temperature (RT) ILs, suitable for electrochemical double layer capacitors (EDLCs) and LIBs, but all of them have been realized utilizing AILs.[9] Polymer electrolytes based on PILs have been used as proton conductive membranes in fuel cells.[10] Trivedi et al. successfully implemented a mixture of protic and aprotic polymeric electrolytes in an activated carbon-based EDLC, whereas Mishra et al. used a PIL-based gel polymer in a proton battery.[11] To the best of our knowledge, however, safe, self-standing, and robust polymer electrolytes encompassing PILs, which are suitable for stable operation in EDLCs and LIBs, have not been reported. Nevertheless, the development of these polymer electrolytes could be interesting for several reasons. First of all,

T. Stettner, Prof. A. Balducci
Institute for Technical Chemistry and Environmental Chemistry
Center for Energy and Environmental Chemistry Jena (CEEC Jena)
Friedrich Schiller University Jena
Philosophenweg 7a, 07743 Jena, Germany
E-mail: andrea.balducci@uni-jena.de

G. Lingua, M. Falco, Prof. C. Gerbaldi
GAME Lab
Department of Applied Science and Technology (DISAT)
Politecnico di Torino
C.so Duca degli Abruzzi, 24-10129 Torino, Italy
E-mail: claudio.gerbaldi@polito.it

The ORCID identification number(s) for the author(s) of this article can be found under https://doi.org/10.1002/ente.202000742.



**DOI: 10.1002/ente.202000742**

the immobilization of PILs inside of a polymer network would reduce the risk of leakage typical for other liquid electrolytes, thus further improving the safety of systems and their cycle life. In addition, the use of polymer electrolyte membranes could enable the use of PILs in flexible and/or shapeable storage systems. Finally, the use of a solid electrolyte incorporating a PIL could also be a strategy to overcome the limitation related to the high reactivity of these ILs toward alkali metals, which is presently hindering the practical use of PIL-based electrolytes in high energy/power density alkali metal batteries, thus limiting the field of application of this family of electrolyte. This latter aspect appears particular interesting, because the direct use of lithium metal would make the use of PIL in the next generation of high-energy density batteries possible, e.g., Li–S and Li–air.

In this work, we propose the use of PIL-based polymer electrolytes suitable for application in energy storage devices. In particular, we studied a novel polymer electrolyte based on UV-crosslinked poly(ethylenoxide) (PEO), encompassing the PIL 1-butylpyrrolidinium bis(trifluoromethanesulfonyl)imide ($Pyr_{H4}TFSI$) and lithium bis(trifluoromethanesulfonyl)imide (LiTFSI). In the first part of the manuscript, the ionic conductivity, thermal properties, and electrochemical stability of this novel polymeric electrolyte are investigated. In the second part of this study, we demonstrate, for the first time, that the PIL-based crosslinked polymer electrolytes can be successfully used for the realization of solid EDLCs and solid lithium-metal batteries, able to display high performance at RT.

## 2. Results and Discussion

### 2.1. Chemical–Physical Characterization

The crosslinked PEO-based polymer electrolyte encompassing PyrH4TFSI, namely PEO_HPyr, was prepared by a simple, green, solvent-free procedure. It includes a hot-pressing step (15 min) for film formation and a rapid (6 min) free-radical reaction induced by UV light (UV curing) to crosslink the network. This results in an easy-to-handle, ready-to-use electrolyte membrane. The polymer electrolyte contains equal amounts by weight of PEO and $Pyr_{H4}TFSI$ (i.e., 41%), 16% of LiTFSI, and 2% of benzophenone (BP) as the hydrogen abstraction photoinitiator.

The crosslinking step, which is sketched in **Figure 1**A, allows obtaining a transparent, self-standing film, which is elastic and shape retaining, as shown in Figure 1B. As previously demonstrated, the crosslinking step is fundamental to obtain amorphous, highly ionic conductive PEO-based electrolytes encompassing high amount of IL without any leakage, while keeping good mechanical properties and integrity.[10a,12]

The scanning electron microscope (SEM) images, energy-dispersive X-ray spectroscopy (EDX) mapping and surface profile analysis indicate that these membranes are highly homogeneous (Figure S1 and S2, Supporting Information). More in-depth field emission scanning electron microscopy analysis was performed to characterize the morphology of the photocured polymer electrolytes. Representative microscopy images are shown in **Figure 2**, which were taken from a cross-sectional view to better show the morphology of the crosslinked samples. As already reported in previous studies,[13] the surface of the

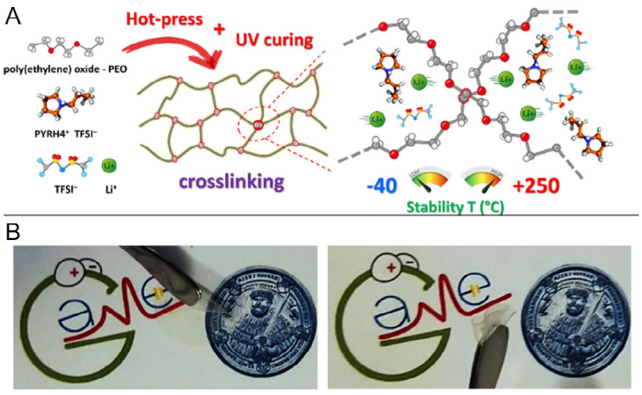


**Figure 1.** A) Schematics of materials, polymer electrolyte preparation, and crosslinking at different magnifications with indication of the temperature range of stability. B) Digital photographs of the PEO_HPyr polymer electrolyte membrane under investigation, showing excellent robustness and elasticity even well above the melting temperature of PEO.

polymer electrolyte shows uniform wrinkled textural features, due to crosslinking of the PEO chains under UV light in the presence of BP. Within these, amorphous PEO domains are alternated to some residual-ordered (semi-crystalline) domains. In case the same precursor mixture is processed without final UV irradiation, the resulting sample shows nonuniform and hardly homogeneous texture (inset of Figure 2b). Conversely, UV-induced crosslinking allows encompassing high amount of PIL and salt, leading to a material with dramatically different morphological characteristics in terms of homogeneity and robustness. Here, the amorphous UV-cured PEO-based network is able to efficiently hold the PIL without any leakage (see, in particular, the previous study[12]).

The prepared PEO_HPyr displays a flash point higher than 300 °C, and when exposed to an open flame, they do not catch fire (Figure S3, Supporting Information).

**Figure 3** compares the thermal stability of the neat $Pyr_{H4}TFSI$ of the binary mixture LiTFSI:$Pyr_{H4}TFSI$ (1:4 molar ratio, indicated as HPyr) and PEO_HPyr. As shown in Figure 3A, the thermal stability of the three electrolytes is very similar, and all of them start to decompose around 300 °C. Above this temperature, the liquids are steadily decomposing, whereas HPyr shows an increased stability compared with pure $Pyr_{H4}TFSI$. This can be attributed to the presence of LiTFSI, a salt with a higher thermal stability, in the former. The polymer electrolyte membrane behaves differently. As shown in Figure 3A, it displays a distinct decomposition between 300 and 330 °C. The weight loss in this temperature range can be attributed to the decomposition of $Pyr_{H4}TFSI$, which is accounting for roughly 40% of the total mass of PEO_HPyr. Above 330 °C, PEO starts to decompose, and at 460 °C, only lithium compounds, e.g., lithium oxide and other non-volatile residues, are left. Figure 3B shows the thermal stability of PEO_HPyr during isothermal measurements carried out at 60 °C for 24 h under nitrogen (blue) and oxygen (black) atmosphere. In these conditions, the polymer electrolyte membrane is extremely stable, and it only loses 1–2% of its initial weight. This minor loss, however, is due to the residual water, which was absorbed prior

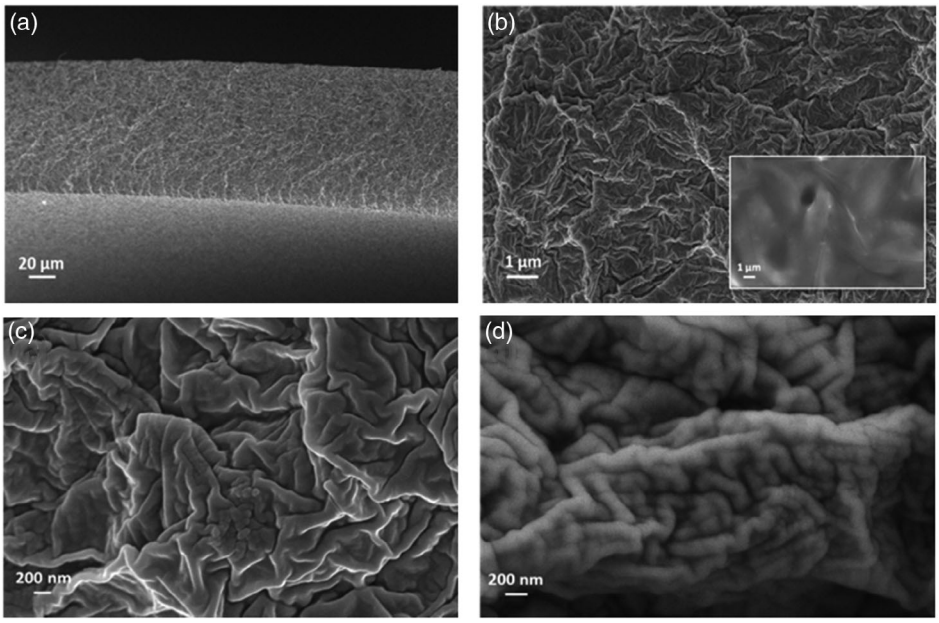


**Figure 2.** a–d) SEM images of the crosslinked PEO_HPyr polymer electrolyte, showing its microstructure at increasing magnification; the inset of (b) show the appearance of a non UV-crosslinked polymer electrolyte obtained with the same precursor mixture.

to the test, as the different preparation steps are carried out under controlled atmosphere and using only battery grade and/or carefully dried materials.

**Figure 4** shows a comparison of the variation of conductivities at different temperatures of neat $Pyr_{H4}TFSI$, HPyr, and PEO_HPyr. As shown, neat $Pyr_{H4}TFSI$ displays a conductivity of 3.5 mS cm$^{-1}$ at 30 °C. Below this temperature, however, this PIL does not display any practical conductivity due to its crystallization. HPyr, which is a binary mixture of $Pyr_{H4}TFSI$ and LiTFSI, displays a lower conductivity compared with the neat PIL (1.3 mS cm$^{-1}$ at 30 °C) but, at the same time, a larger temperature range in which the electrolyte is displaying a decent conductivity (0.03 mS cm$^{-1}$ at 10 °C), due to the melting point decrease induced by LiTFSI. The ionic conductivity of PEO_HPyr at 30 °C is 0.14 mS cm$^{-1}$, which is a high value for a solid polymer electrolyte, especially near RT.[10c] Considering these results, the practicable temperature window of PEO_HPyr is wider compared with the liquid electrolytes, which represents a substantial advantage offered by the polymer electrolyte. The fully amorphous character of the film obtained by the UV-induced crosslinking of the macromolecular chains is demonstrated by the lack of a clear change in an activation energy at 40–60 °C, which is generally observed with typical semi-crystalline PEO-based electrolytes, obtained by standard solvent casting and/or hot-pressing, due to the phase transition of crystalline PEO.[10a,10b] This result is consistent with the differential scanning calorimetry (DSC) measurement (Figure S4A, Supporting Information), where no obvious melting or crystallization peaks are observed. Similarly, other literature reports about crosslinked PEO-LiTFSI-ILs films show that the crystallization of PEO and P(EO)$_n$LiTFSI complexes can be hindered in these ternary electrolytes.[14] Nevertheless, in these systems, the crystallization of excess IL may occur depending on the composition.[14c] In the present work, this latter phenomenon was not observed by either SEM or DSC analyses. The ionic conductivity shows a Vogel–Tamman–Fulcher (VTF) dependence typical of fully amorphous polymer electrolytes.[14b,14c] The VTF plot of the logarithm of conductivity versus $(T–T_0)^{-1}$ for PEO_HPyr is shown in Figure S4B, Supporting Information. Figure S5, Supporting Information, shows the VTF plot of the ionic conductivity of $Pyr_{H4}TFSI$ and HPyr. The apparent activation energy ($E_a$) can be extracted from the linear interpolation of the ionic conductivity data according to Equation (1)[15]

$$\ln \sigma = A + \frac{E_a}{R(T - T_0)} \quad (1)$$

Here, $A$ is a factor depending on the ionic conductivity at infinite temperature, $R$ is the universal gas constant, and $T_0$ is a parameter customarily located 30 K below the glass transition temperature ($T_g$), which is related to the zero configurational entropy of the system.[15] On the basis of the first DSC heating scan, $T_g$ is located at −50.7 °C. From the linear fit, apparent $E_a$ values of 4.8, 5.4, and 7.0 kJ mol$^{-1}$ have been calculated for $Pyr_{H4}TFSI$, HPyr, and PEO_HPyr, respectively. These values indicate that the $E_a$ of PEO_HPyr is rather comparable to that of the liquid PIL, and it is also similar to that of $Pyr_{14}TFSI$/LiTFSI solutions.[15]

**Figure 5** shows the ESW of the PEO_HPyr at RT (scan rate of 0.1 mV s$^{-1}$). The crosslinked PEO_HPyr electrolyte displays an overall ESW of ≈3.5 V (with cathodic and anodic limits of −0.9 and 2.6 V versus Ag, respectively). This value is lower than that observed for many AIL-based polymeric electrolytes, but is comparable to that of the liquid PIL (see Figure S6, Supporting Information), indicating that the immobilization of $Pyr_{H4}TFSI$ in a PEO matrix is not significantly affecting the electrochemical stability of this PIL.

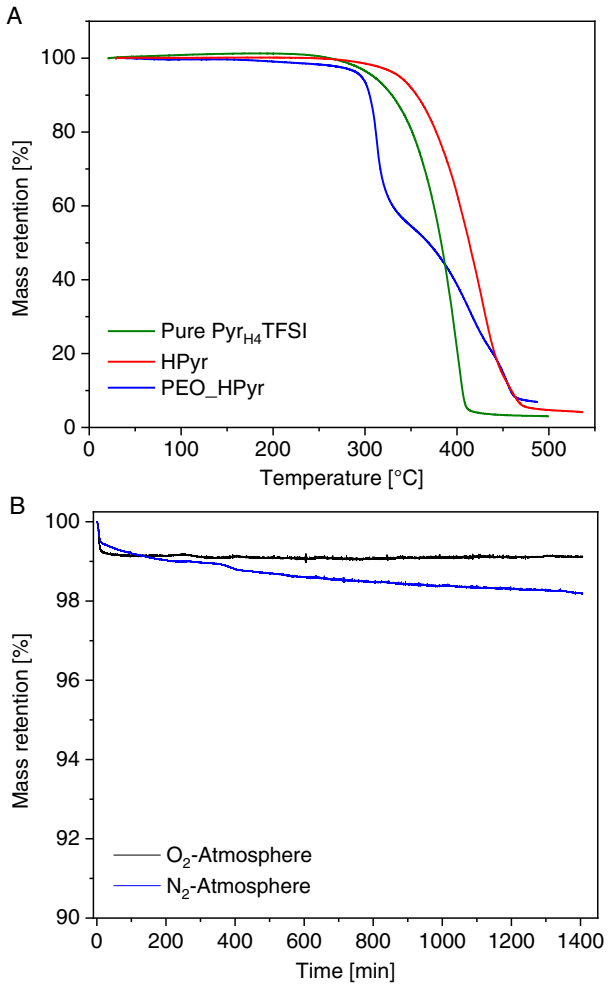


**Figure 3.** A) TGA of pure $Pyr_{H4}TFSI$, HPyr, and PEO_HPyr heated at 10 °C min$^{-1}$. B) Isothermal (60 °C) mass loss of PEO_HPyr under $O_2$ and $N_2$ atmosphere, respectively.

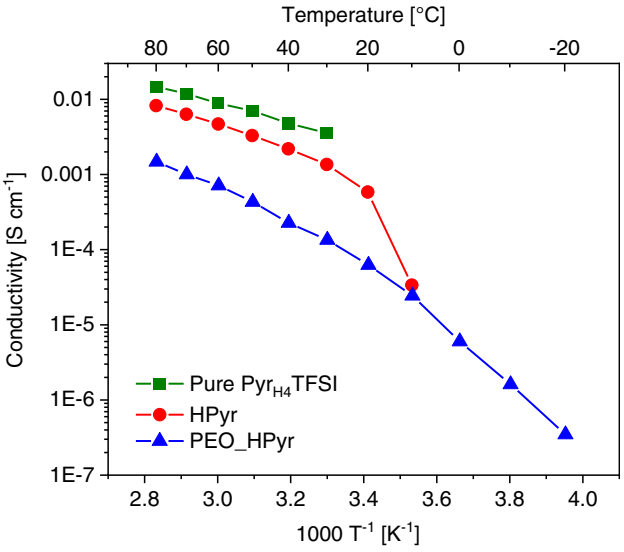


**Figure 4.** Arrhenius plot of the ionic conductivity in the range of −20 to 80 °C of the crosslinked PEO_HPyr polymer electrolyte compared with HPyr liquid electrolyte and neat $Pyr_{H4}TFSI$.

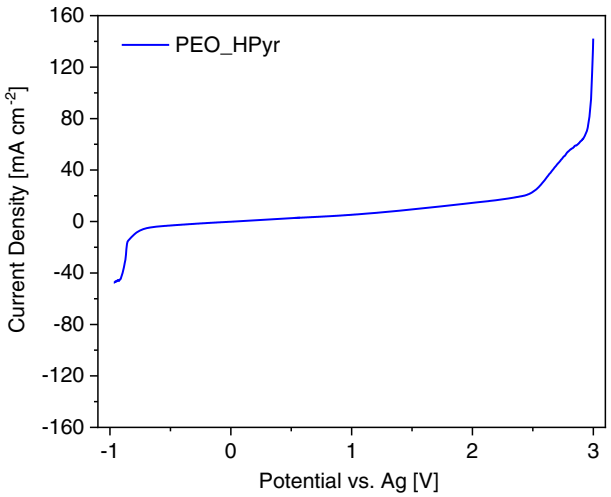


**Figure 5.** ESW of the polymer electrolyte (PEO_HPyr), measured via linear sweep voltammetry with a platinum working electrode, silver reference electrode, and an oversized carbon counter electrode at 40 °C and 0.1 mV s$^{-1}$.

Considering these results, the PEO_HPyr appears as an electrolyte with an interesting set of transport, thermal, and electrochemical properties. These properties are making this crosslinked PIL-based solid polymer electrolyte suitable for the realization of electrochemical energy storage devices operating at RT.

### 2.2. All-Solid PEO_HPyr-Based EDLCs

At first, the PEO_HPyr was used for the realization of a proof-of-concept lab-scale all-solid EDLC containing activated carbon-based electrodes and having an operating voltage of 2 V. This operating voltage was selected, because it is safely achievable with the liquid HPyr.[6] As shown in the cyclic voltammogram (CV) in **Figure 6**A, this all-solid EDLC displays a capacitive-like behavior without any signs of irreversible redox reactions. Clearly, due to the limited electrolyte conductivity, the system shows a rather high resistance, as visible in the constant current (CC) (galvanostatic) charge/discharge voltage profiles versus time in Figure 6B. Nevertheless, this resistance appears comparable with that observed with other ILs (both protic and aprotic), and it is certainly acceptable for a lab-scale device, especially considering that the EDLC under study is solid state and has been tested at RT.[16]

With the aim to investigate the overall performance of the all-solid EDLC, also CC tests at different current density rates and float tests at different voltages have been carried out. **Figure 7**A shows the behavior of the EDLC under study during 1200 CC cycles carried out at different current densities. During the initial 100 cycles at 1 mA g$^{-1}$, the capacitance of the device is constantly increasing, and this increase becomes more marked when the current density is reduced to 0.5 mA g$^{-1}$ (cycles 100–200).

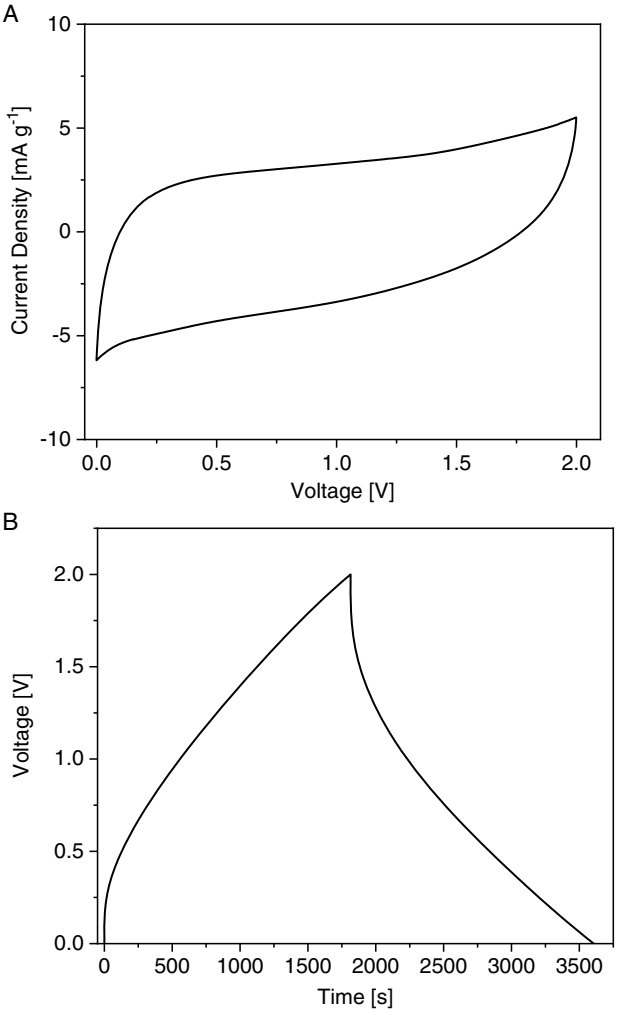


**Figure 6.** A) CV at 0.5 mV $s^{-1}$ and B) CC curve at 1 mA $g^{-1}$ of an activated carbon-based EDLC using PEO_HPyr.

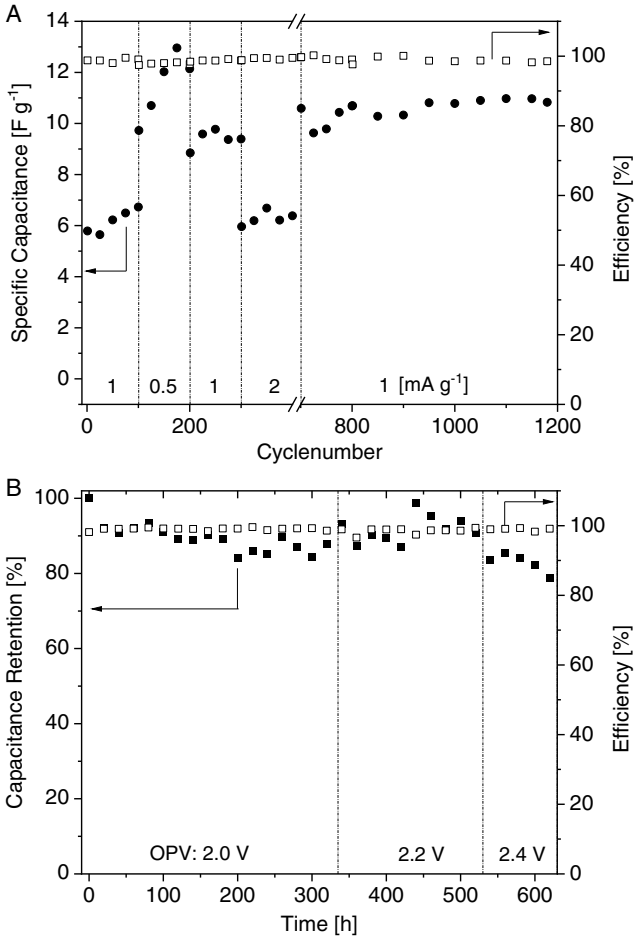


**Figure 7.** A) Rate capability test performed via CC measurements at different current densities and B) float test at different operative voltages of an activated carbon-based EDLC using PEO_HPyr at 1 mA $g^{-1}$.

This behavior is typical for highly viscous electrolytes, e.g., ILs, and it has been reported in the literature several times.[16d,17] An optimization of the electrode/electrolyte interface, as well as of the charge protocol/conditions, could reduce the time needed for this activation process. Nevertheless, this kind of optimization is out of the scope of this work and, therefore, was not carried out.[17,18] It is very important to notice that the all-solid EDLC is able to deliver a capacitance of 12 F $g^{-1}$. By comparison, a device with the same electrodes used in combination with a PIL-based liquid electrolyte is able to deliver a capacitance of 18–20 F $g^{-1}$.[6,16b] Considering the fact that the investigated system was not optimized (see below) and it was an all-solid EDLC, the capacitance delivered by the investigated devices under the applied operative conditions can certainly be considered as very promising. Due to the limited electrolyte conductivity, the capacitance retention of the investigated EDLC during tests at higher current densities is limited, and the system is able to deliver a moderate capacitance of 6 F $g^{-1}$ only up to 2 mA $g^{-1}$. Above this latter value, the capacitance drops significantly, although the system provides a stable behavior (cycles 400–700, not shown). After the rate capability test at different current densities, the all-solid EDLC was cycled for over 500 cycles at 1 mA $g^{-1}$, and it showed a very good cycling stability, with a constant capacitance of ≈10 F $g^{-1}$. To gain a better understanding of the stability of this innovative EDLC, after the CC tests, also float tests were carried out (Figure 7B). Initially, the voltage of the EDLC was held at 2 V. As shown in the figure, after 340 h at this voltage, the all-solid EDLC device was able to keep 90% of its initial capacitance. Afterward, the cell voltage was increased to 2.2 V, which is the maximal operative voltage possible using liquid HPyr. Even at this voltage, the all-solid EDLC displays a very high stability for 240 h with a capacitance retention of 90%. Finally, the cell voltage was increased to 2.4 V. At this voltage, the device with PEO_HPyr is less stable, and its capacitance decreases faster, dropping already after 50 h below 80% of its initial capacitance. The same behavior is observed with liquid HPyr.[6] It is important to remark that at an industrial level, one of the stability targets of EDLCs is to display a capacitance retention of 80% after 500 h of float at the maximum operative voltage.[16a] Considering the results of the float test, the investigated all-solid EDLC, although not optimized, appears to display

a very remarkable stability. It is also worth mentioning that the Nyquist plots of the device are not drastically changing during the float test (see Figure S7, Supporting Information).

Overall, the results reported earlier are very interesting, as the all-solid-state EDLC displays good capacitance and high cycling stability, the latter even higher compared with an EDLC operating with liquid HPyr.[6] Combined with the general advantages of an all-solid-state EDLC, such as no risk of leakage, compactness, and the possibility for the design and realization of flexible devices, they appear even more attractive. It is also important to remark that these results were obtained using electrodes with a rather high mass loading (2.6–3.5 mg $cm^{-2}$) for a solid-state system, that the investigated devices were not optimized (e.g., in terms of electrode balancing and electrode–electrolyte surface), and that all the tests were carried out at RT. Considering these points, it is reasonable to suppose that the performance of the investigated systems can be significantly improved in the near future. Work is in progress to realize an optimized all-solid EDLC.

### 2.3. All-Solid PEO_HPyr-Based Lithium-Metal Cell

As expected, considering the ESW of liquid HPyr, deprotonation of the $[Pyr_{H4}]^+$ cation, followed by the electrolyte degradation and hydrogen evolution upon reduction at the Li-metal anode, results in an irregular voltage profile during the first charge and cell failure in four CC cycles in a Li/PEO_HPyr/lithium iron phosphate (LFP) cell at C/10 rate and RT (Figure S8, Supporting Information).[10d] Preventing the direct contact of the anode with the PIL is fundamental to avoid hydrogen evolution. The confinement of the PIL in the crosslinked polymer matrix is not 100% sufficient to avoid this phenomenon; therefore, an effective protective layer on Li metal is fundamental to enable cycling with PILs. In this regard, vinylene carbonate (VC) was, herein, experimented as an additive to allow the formation of the Li-metal protective layer.

The use of VC as an additive is widespread in LIB electrolytes.[10d] This cyclic carbonate bears a double bond, allowing the formation of a protective layer on the anode upon electrochemical reduction during the first charge. This process occurs at relatively high potentials versus $Li^+/Li$ as compared with the other components in the common electrolytes, promoting the formation of a passivation layer, which avoids further undesired decomposition reactions.[10d]

As a preliminary test to check the effectiveness of a VC-based layer to prevent the decomposition of the PIL, a film of poly(vinylene carbonate) was obtained from VC upon a free radical-induced polymerization triggered by azobisisobutyronitrile (AIBN). The film was weighed and then swelled in the PIL overnight. No weight change could be detected after swelling, confirming that the uptake of the liquid phase was negligible. Thus, VC-based films qualitatively proved to be good candidates for preventing the diffusion of $[Pyr_{H4}]^+$ toward the Li-metal anode. As PEO_HPyr is obtained by a free radical crosslinking process, the simple addition of VC in the PIL-based polymer electrolyte mixture would result in the grafting/polymerization of VC, thus preventing the formation of an effective VC-based protective film on lithium metal.[11b]

Therefore, here, we prepared a proof-of-concept lab-scale solid-like Li-metal cell in which the surface of the lithium-metal electrode was wetted with few drops of a solution of $Pyr_{H4}TFSI$ and LiTFSI (having a PIL:salt molar ratio equal to 4:1) added with 10% by weight of VC prior to contacting the crosslinked PEO_HPyr polymer electrolyte and stacking the cell components in a standard sandwiched Li/PEO_HPyr-VC/LFP configuration. The cell was cycled at C/20 and C/10 rate (i.e., ≈0.01 and 0.02 mA $cm^{-2}$, respectively), based on the content of LFP active material (AC) and its theoretical capacity (170 mAh $g^{-1}$) at RT (**Figure 8**A). Differently from the cell with the PEO_HPyr alone, flat voltage profiles typical for LFP are observed, with a rather limited overpotential (below 100 mV at C/20 rate), considering the amount of VC used to prepare the swelling solution, the thickness of the polymer electrolyte (≈120 μm), and that the cell was cycled at RT. The coulombic efficiency of the first cycle is 97.5%, probably limited by processes occurring at the interface

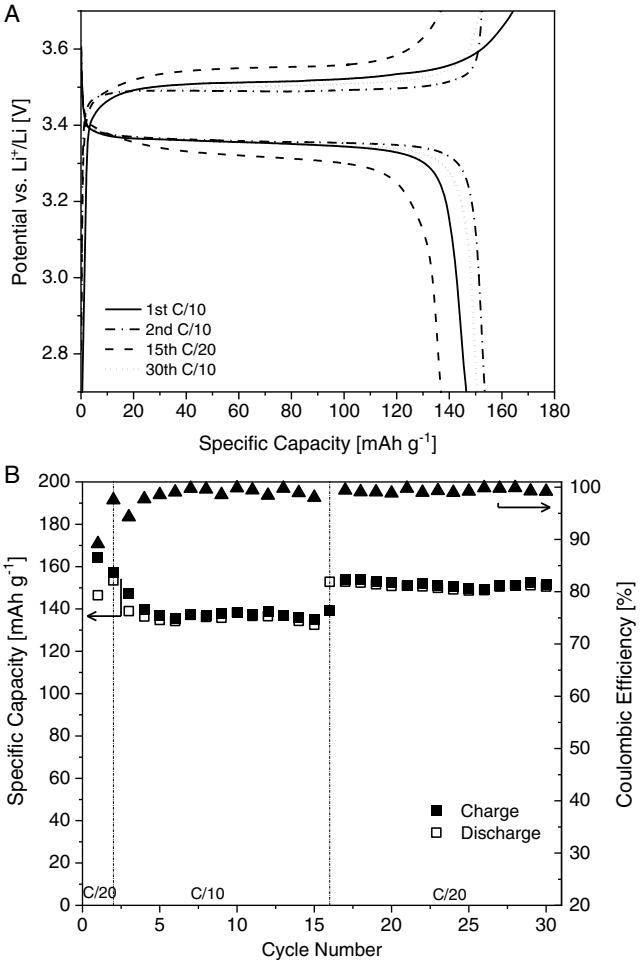


**Figure 8.** A) Voltage profile versus specific capacity during CC cycling of a Li/PEO_HPyr-VC/LFP cell at C/20 and C/10 rate and RT. B) Specific capacity and coulombic efficiency versus cycle number upon CC cycling of the proof-of-concept lab-scale solid-like Li/PEO_HPyr-VC/LFP Li-metal cell in which the surface of the lithium-metal electrode was wetted with few drops of a solution of $Pyr_{H4}TFSI$ and LiTFSI (having a PIL:salt molar ratio equal to 4:1) added with 10% by weight of VC prior to contacting the crosslinked PEO_HPyr polymer electrolyte.

electrolyte/electrode, including the formation of the protective layer on the Li-metal surface promoted by the presence of VC. By the second cycle at C/10 rate onward, the coulombic efficiency increases, reaching values ≥98.5 and ≥99.2% at C/10 and C/20 rate, respectively, which accounts for the high reversibility of the charge/discharge processes. The specific discharge capacity at C/20 rate is 154 and 151 mAh $g^{-1}$ after 2 and 30 cycles, respectively. These values are close to the practical specific capacity of the LFP used in this work, which is about 158 mAh $g^{-1}$.[11a] At C/10 rate, the specific discharge capacity delivered by the cell is about 136 mAh $g^{-1}$, and the overpotential is about 200 mV, due to the clear limitations associated with the internal resistance of the cell, which can be decreased upon further optimization beyond the scope of this article. Nevertheless, it is important to remark that the performance of this proof-of-concept cell, being the first example of a PIL-based solid polymer electrolyte operating with a Li-metal electrode, is already comparable with that reported for cells with analogous electrodes (in our case, in addition, we used a standard LFP electrode, without any ion conductive binder) and solid electrolytes based on AILs (see Table S1, Supporting Information, for a more detailed comparison).

Future work will be dedicated to the investigation of the protective layer formed by VC on the surface on the Li-metal surface and the modification of the preparation procedure of the polymer electrolyte, to directly incorporate the proper quantity of VC in the reaction mixture and obtain a thin film enabling cell operation at higher current densities.

## 3. Conclusion

This work reports, for the first time, about the preparation and characterization of a crosslinked polymer electrolyte encompassing $Pyr_{H4}TFSI$/LiTFSI PIL-based mixture and its effective use at ambient conditions in lab-scale EDLCs and, for the very first time, in proof-of-concept lithium-metal batteries. We have shown that this novel solid electrolyte displays elasticity, robustness, and safety due to non-flammability, along with high ionic conductivity at low temperature and thermal stability in a wide temperature range. As in the case of liquid PILs, the ESW of the polymer electrolyte is limited by the acidic proton in the PIL. Nevertheless, this is not hindering the application of this innovative solid electrolyte in energy storage devices.

Indeed, we realized the first example of an all-solid-state EDLC operating with the crosslinked PEO_HPyr-based electrolyte. We have shown that this device displays excellent performance in terms of capacitance output at RT, comparable to that achievable with the liquid PIL. This performance is coupled with largely enhanced stability, in addition to the advantages listed in the previous paragraph. Offering the typical benefits of an all-solid system such as flexibility, compactness, and improved safety (no risk of leakage), this unoptimized system appears already very attractive not least due to the larger temperature range in which it can be utilized, compared with the liquid PIL.

Furthermore, we presented the first example of a PIL-based lithium-metal battery assembled with an LFP cathode and a Li-metal anode. This proof-of-concept system has been realized by protecting the Li-metal anode with a VC-containing electrolyte, which is electrochemically polymerized during the initial charge. The system displayed almost full specific capacity output and stable cycling at different current rates at RT. The use of a solid electrolyte incorporating a PIL appears, therefore, as a feasible strategy to suppress the high reactivity of these ILs toward alkali metals, and to allow the introduction of PIL-based electrolytes in metal batteries.

International developments at European Union (EU) level and abroad to reduce air pollution and $CO_2$ production are pushing toward a rapid implementation of electrification of transport, and the rush for better technology correspondingly necessitates improved, safe traction battery systems operating in a broad temperature range. In this respect, stable, low-cost, all-solid-state lithium-metal batteries are a key enabling technology providing high energy/power density output, which can easily be coupled with all-solid-state EDLC in an integrated architecture for even enhanced performance. The results of this study clearly enlighten that PIL-based crosslinked polymer electrolytes are a new and very interesting class of safe, stable, low-cost solid electrolytes that can definitely serve the purpose. Clearly, we are still at the proof-of-concept stage, and in the near future, additional efforts will be needed to understand the properties of these solid electrolytes, e.g., ion mobility, and their interactions with the electrode materials to further improve the performance of PIL-based systems.

## 4. Experimental Section

*Synthesis of the IL*: The PIL was synthesized with a procedure similar to that reported in a previous study.[19] In a first step, 10.55 g of the yellowish precursor 1-butylpyrrolidine (98%, obtained by *Aldrich*) was distilled at 60 °C and 20 mbar. After the distillation, colorless 1-butylpyrrolidine (7.55 g/59.34 mmol) was put in a two-neck flask on a magnetic stirring plate. The flask was topped by a reflux condenser and a 50 mL dropping funnel, which was filled with 5.35 mL HCl (35%).

HCl was added dropwise and slowly under stirring, while the mixture was cooled with an ice bath. After the complete addition, the ice bath was removed, and the solution was stirred for 2 h. Residual water and reactants were removed under reduced pressure, leaving 1-butylpyrrolidine chloride as a solid.

The 1-butylpyrrolidine chloride was solved in 8 mL of $H_2O$ and then put into a two-neck flask, equipped with a reflux condenser and a 50 mL dropping funnel; 19.33 g of LiTFSI (99.95%, obtained by *Aldrich*) was solved in 18 mL of $H_2O$ and filled into the dropping funnel. The LiTFSI solution was added to 1-butylpyrrolidine dropwise, and the mixture was stirred for 3 h. During this reaction, two phases were formed: an organic one containing $Pyr_{H4}TFSI$, at the bottom and an aqueous one on top. To remove the aqueous from the organic one, a separating funnel was used.

Subsequently, the PIL was washed five to six times with water, to remove residual LiCl. To test on complete removal, $AgNO_3$ was added to the washing water.

As a last step, residual water was removed by reduced pressure and heating (60 °C, $3.0 \times 10^{-3}$ mbar).

*Preparation of the Polymer Electrolyte*: To prepare the polymer electrolytes, LiTFSI (*Solvionic*, battery grade) was first carefully mixed with PEO (Mn 200 000 Da, *Merck*, dried under vacuum at 55 °C for two days prior use), and the mixture was melt and mixed at 80 °C until complete homogenization, resulting in a highly viscous paste. The solution of the photoinitiator BP (*Merck*) dissolved in $Pyr_{H4}TFSI$ was then added to the paste. Continuous mixing at 80 °C yielded homogeneous blends. The weight percentages of PEO, $Pyr_{H4}TFSI$, LiTFSI, and BP are 41, 41, 16, and 2 wt%, respectively. The molar ratio among the components PEO:$Pyr_{H4}TFSI$:LiTFSI is approximately 16.7:1.7:1. The operations mentioned earlier were

carried out in an argon filled glove box (Jacomex GP concept, <1 ppm $H_2O$ and <1 ppm $O_2$). The blend was then processed into a film by hot-pressing for 15 min at 10 bar and 70 °C between two polypropylene sheets with adhesive tape as spacers in sealed bags and crosslinked upon irradiation by UV light (UV curing) for 6 min at 40 mW cm$^{-2}$ using a medium-pressure Hg lamp (*Helios Quartz*).

*Scanning Electron Microscope*: The SEM pictures were taken and EDX mapping done using a *pro X* from *PhenomTM*.

*Surface Profile*: The surface profile was measured using a *Zeiss SmartProof 5* profilometer. The calculations were done using the software *ZEN smartproof* by *Zeiss*.

*Thermogravimetric Analysis*: The thermogravimetric analysis (TGA) was performed with a *PerkinElmer STA 6000* using nitrogen or oxygen as carrier gas with a total flow rate of 20 mL min$^{-1}$. For each measurement, about 15 mg of solid or liquid electrolyte was filled in a platinum crucible. For TGA measurements, the samples were heated to 500 °C with a gradient of 10 °C min$^{-1}$. For isothermal measurements, a gradient of 30 °C min$^{-1}$ was used to reach 60 °C, which was hold for 24 h.

*Electrochemical Measurements*: In all cases, the cells with the self-standing crosslinked polymer electrolytes were assembled without any additional spacer or separator. The proof-of-concept lab-scale solid-like Li-metal cell was assembled, placing the polymer electrolyte membrane directly in contact with the lithium-metal anode, whereas the other side was placed in contact with the LFP electrode disk, stacking the cell components in a standard sandwiched configuration. For the Li-metal cell with Li/PEO_HPyr-VC/LFP configuration, we followed the same procedure reported earlier, with the addition of pre-treatment on the anode: the surface of the lithium-metal electrode was wetted with few drops of a solution of $Pyr_{H4}$TFSI and LiTFSI (having a PIL:salt molar ratio equal to 4:1) containing 10% by weight of VC prior to contacting the crosslinked PEO_HPyr polymer electrolyte. The cells with liquid electrolyte were equipped with glass microfiber filters (*Whatman,* 150 µm) as separators, drenched with 150 µL electrolyte. All cells were assembled in an argon filled glove box (*MBraun LABmasterpro ECO glove boxes*, <1 ppm $H_2O$ and <1 ppm $O_2$).

The ionic conductivity of the polymer electrolyte was evaluated from the impedance response of the symmetric cells (*ECC*-Std cells by EL-*CELL GmbH*) assembled by sandwiching PEO_HPyr between two stainless steel (SS-316) blocking electrodes. The impedance spectra were recorded at an oscillating voltage of 10 mV in the frequency range between $3 \times 10^5$ and 1 Hz, using a *VMP3* electrochemical workstation (*Biologic*). The test was carried out while increasing the temperature in 10 °C steps from −20 to 80 °C using an environmentally controlled climate chamber (*BINDER, MK53 E2*). The cell was kept for at least 90 min at each given temperature for proper equilibration. The impedance spectra were analyzed using the *ECLab* V10.44 software. The bulk resistance ($R_b$) was extracted from the intercept (on the real impedance axis) of the signal due to the double layer capacity at the blocking electrodes. The ionic conductivity ($\sigma$) was calculated using Equation (2)

$$\sigma = \frac{t}{R_b * } \tag{2}$$

The thickness ($t$) of the samples is the average of three measurements carried out with a micrometer (*Mitutoyo* gauge). The area ($A$) of the samples is 2.54 cm$^2$.

The ESW of the electrolytes was measured in a three-electrode *Swagelok* cell using a platinum working electrode, an oversized activated carbon electrode as the counter electrode, and a silver pseudo-reference electrode. Activated carbon electrodes were prepared following a procedure identical to that used by Krause et al.[20] The dry composition of the electrodes is 90 wt% of AC (*DLC Super*, *Norit*), 5 wt% of conducting agent (*Super C65*, *Imerys*), and 5 wt% of binder (carboxymethyl cellulose, *Dow*). The mass loading of the electrodes is between 2.6 and 3.5 mg cm$^{-2}$, and the electrode area equals to 1.13 cm$^2$. After a 12-h open circuit voltage (OCV) measurement to reach equilibrium, the cells were swept from OCV toward either positive or negative direction at 0.1 mV s$^{-1}$ until a potential of −6 V versus OCV and 6 V versus OCV was reached, respectively. These measurements were carried out at 40 °C, both for the liquid as well as for the solid electrolyte, to ensure the former to be molten while keeping the results comparable.

The electrochemical behavior of the EDLCs at RT was evaluated in a three-electrode *Swagelok* cell using activated carbon electrodes prepared as described earlier. The cyclic voltammetry measurements were carried out at different scan rates (0.5, 1, 5, 2.5, and 10 mV s$^{-1}$), and the CC experiments were carried out at different current densities (0.1, 0.5, 1, 2, 5, and 10 mA g$^{-1}$). The stability tests were also performed via CC measurements with a specific current of 1 mA g$^{-1}$. First, 5000 CC cycles were executed. For the float tests, only 50 cycles were measured but with a 20 h period of holding the cell at its designated operative voltage afterward. This was repeated until a period of roughly 600 h at the maximum voltage was reached, calculating the capacitance after each 50th cycle of the CC step.

Lab-scale cells with Li-metal anodes and LFP cathodes were assembled by simply sandwiching the components in ECC-Std cells (*EL-Cell GmbH*). The area of LFP (*Clariant-LP2*) and Li-metal (200 µm, *Chemetall*, now *Albemarle*) electrodes is 2.54 cm$^2$. CC tests were carried out with an *ARBIN BT2000* battery tester. The cutoff voltage values were set to 2.7 and 3.7 V versus $Li^+$/Li. The cathodes were prepared by a standard method from an *N*-methyl pyrrolidone (NMP; *Merck*) slurry containing LFP, conductive carbon (*Shawinigan Black AB50*, *Chevron Corp*), and polyvinylidene fluoride (Mn 534000, *Merck*) at 70:20:10 weight ratio, respectively. The slurry was deposited onto an Al foil, dried overnight, cut into disks, and vacuum dried at 120 °C for one day prior use to remove water and residual NMP. The resulting AC loading is about 1.0 mg cm$^{-2}$.

## Supporting Information

Supporting Information is available from the Wiley Online Library or from the author.

## Acknowledgements

T.S. and A.B. wish to thank the Friedrich-Schiller University for the support. C.G., M.F., and G.L. acknowledge financial support by the Si-DRIVE Project, which received funding from the EU's Horizon 2020 research and innovation program under GA 814464. Open access funding enabled and organized by Projekt DEAL.

## Conflict of Interest

The authors declare no conflict of interest.

## Keywords

electrochemical capacitors, lithium-metal batteries, polymer electrolytes, protic ionic liquids, solid-state devices

Received: August 21, 2020
Published online:

[1] a) M. Anouti, M. Caillon-Caravanier, Y. Dridi, H. Galiano, D. Lemordant, *J. Phys. Chem. B* **2008**, *112*, 13335; b) D. M. Fox, J. W. Gilman, A. B. Morgan, J. R. Shields, P. H. Maupin, R. E. Lyon, H. C. De Long, P. C. Trulove, *Ind. Eng. Chem. Res.* **2008**, *47*, 6327; c) H. Sun, G. Zhu, X. Xu, M. Liao, Y.-Y. Li, M. Angell, M. Gu, Y. Zhu, W. H. Hung, J. Li, *Nat. Commun.* **2019**, *10*, 1.

[2] a) M. A. Susan, M. Yoo, H. Nakamoto, M. Watanabe, *Chem. Lett.* **2003**, *32*, 836; b) H. Nakamoto, M. Watanabe, *Chem. Commun.* **2007**, *24*, 2539–2541.

[3] a) L. Timperman, H. Galiano, D. Lemordant, M. Anouti, *Electrochem. Commun.* **2011**, *13*, 1112; b) X. Lu, G. Burrell, F. Separovic, C. Zhao, *J. Phys. Chem. B* **2012**, *116*, 9160; c) N. Böckenfeld, M. Willeke, J. Pires, M. Anouti, A. Balducci, *J. Electrochem. Soc.* **2013**, *160*, A559.
[4] a) T. Vogl, C. Vaalma, D. Buchholz, M. Secchiaroli, R. Marassi, S. Passerini, A. Balducci, *J. Mater. Chem. A* **2016**, *4*, 10472; b) M. Arnaiz, A. Bothe, S. Dsoke, A. Balducci, J. Ajuria, *J. Electrochem. Soc.* **2019**, *166*, A3504.
[5] T. Vogl, S. Menne, R.-S. Kühnel, A. Balducci, *J. Mater. Chem. A* **2014**, *2*, 8258.
[6] T. Stettner, S. Gehrke, P. Ray, B. Kirchner, A. Balducci, *ChemSusChem* **2019**, *12*, 3827.
[7] P. A. Z. Suarez, C. S. Consorti, R. F. de Souza, J. Dupont, R. S. Gonçalves, *J. Braz. Chem. Soc.* **2002**, *13*, 106.
[8] S. Menne, M. Schroeder, T. Vogl, A. Balducci, *J. Power Sources* **2014**, *266*, 208.
[9] a) Y.-S. Ye, J. Rick, B.-J. Hwang, *J. Mater. Chem. A* **2013**, *1*, 2719; b) S. Chen, K. Wen, J. Fan, Y. Bando, D. Golberg, *J. Mater. Chem. A* **2018**, *6*, 11631; c) F. Ma, Z. Zhang, W. Yan, X. Ma, D. Sun, Y. Jin, X. Chen, K. He, *ACS Sustain. Chem. Eng.* **2019**, *7*, 4675; d) J. R. Nair, F. Colò, A. Kazzazi, M. Moreno, D. Bresser, R. Lin, F. Bella, G. Meligrana, S. Fantini, E. Simonetti, *J. Power Sources* **2019**, *412*, 398; e) E. Simonetti, M. De Francesco, M. Bellusci, G. T. Kim, F. Wu, S. Passerini, G. B. Appetecchi, *ChemSusChem* **2019**, *12*, 4946; f) G. Yang, Y. Song, Q. Wang, L. Zhang, L. Deng, *Mater. Des.* **2020**, *190*, 108563.
[10] a) A. Martinelli, A. Matic, P. Jacobsson, L. Börjesson, A. Fernicola, S. Panero, B. Scrosati, H. Ohno, *J. Phys. Chem. B* **2007**, *111*, 12462; b) S.-Y. Lee, A. Ogawa, M. Kanno, H. Nakamoto, T. Yasuda, M. Watanabe, *J. Am. Chem. Soc.* **2010**, *132*, 9764; c) U. A. Rana, M. Forsyth, D. R. MacFarlane, J. M. Pringle, *Electrochim. Acta* **2012**, *84*, 213; d) Z. Wojnarowska, J. Knapik, M. Díaz, A. Ortiz, I. Ortiz, M. Paluch, *Macromolecules* **2014**, *47*, 4056.
[11] a) K. Mishra, S. Hashmi, D. Rai, *J. Solid State Electrochem.* **2014**, *18*, 2255; b) T. J. Trivedi, D. Bhattacharjya, J. S. Yu, A. Kumar, *ChemSusChem* **2015**, *8*, 3294.
[12] M. Falco, C. Simari, C. Ferrara, J. R. Nair, G. Meligrana, F. Bella, I. Nicotera, P. Mustarelli, M. Winter, C. Gerbaldi, *Langmuir* **2019**, *35*, 8210.
[13] a) J. Nair, L. Porcarelli, F. Bella, *Interfaces* **2015**, *7*, 961; b) L. Porcarelli, C. Gerbaldi, F. Bella, J. Nair, *Sci Rep.* **2016**, *6*, 19892.
[14] a) J.-H. Shin, W. A. Henderson, C. Tizzani, S. Passerini, S..-S. Jeong, K.-W. Kim, *J. Electrochem. Soc.* **2006**, *153*, A1649; b) G.-T. Kim, G. B. Appetecchi, F. Alessandrini, S. Passerini, *J. Power Sources* **2007**, *171*, 861; c) G.-T. Kim, G. B. Appetecchi, M. Carewska, M. Joost, A. Balducci, M. Winter, S. Passerini, *J. Power Sources* **2010**, *195*, 6130.
[15] G. A. Elia, U. Ulissi, F. Mueller, J. Reiter, N. Tsiouvaras, Y. K. Sun, B. Scrosati, S. Passerini, J. Hassoun, *Chem. Eur. J.* **2016**, *22*, 6808.
[16] a) A. Brandt, S. Pohlmann, A. Varzi, A. Balducci, S. Passerini, *MRS Bull.* **2013**, *38*, 554; b) A. Brandt, J. Pires, M. Anouti, A. Balducci, *Electrochim. Acta* **2013**, *108*, 226; c) A. Brandt, A. Balducci, *J. Power Sources* **2014**, *250*, 343; d) F. Béguin, V. Presser, A. Balducci, E. Frackowiak, *Adv. Mater.* **2014**, *26*, 2219.
[17] Z. Lin, E. Goikolea, A. Balducci, K. Naoi, P.-L. Taberna, M. Salanne, G. Yushin, P. Simon, *Mater. Today* **2018**, *21*, 419.
[18] a) N. Handa, T. Sugimoto, M. Yamagata, M. Kikuta, M. Kono, M. Ishikawa, *J. Power Sources* **2008**, *185*, 1585; b) Y. J. Ju, C. H. Lien, K. H. Chang, C. C. Hu, D. S. H. Wong, *J. Chin. Chem. Soc.* **2012**, *59*, 1280; c) J. Krummacher, C. Schütter, L. Hess, A. Balducci, *Curr. Opin. Electrochem.* **2018**, *9*, 64; d) A. Balducci, in *Ionic Liquids II*, Springer, Cham **2017**, pp. 1-27.
[19] L. Timperman, P. Skowron, A. Boisset, H. Galiano, D. Lemordant, E. Frackowiak, F. Béguin, M. Anouti, *Phys. Chem. Chem. Phys.* **2012**, *14*, 8199.
[20] A. Krause, P. Kossyrev, M. Oljaca, S. Passerini, M. Winter, A. Balducci, *J. Power Sources* **2011**, *196*, 8836.